Journal of Dynamics, Energy and Utility

RESEARCH ARTICLE

Impact Performance Comparison of B_4C, Sic, and Al_2O_3 Ceramics With Varying Surface Angles and Velocities

Volkan Arıkan [1*]

[1]Department of Mechanical Engineering, Osmaniye Korkut Ata University, Osmaniye, TÜRKİYE
Corresponding Author *: volkanarikan@osmaniye.edu.tr

Received: 15.04.2025
Accepted: 08.05.2025

Abstract

The paper describes a study on the impact performance of three different ceramic materials with varying surface angles and impact velocities. Finite element analysis was performed to obtain data on projectile residual velocity, absorbed energy values, and damage data on the plates. Boron carbide and silicon carbide showed better impact performance than alumina, and increasing surface angle reduced projectile residual velocity. The amount of absorbed energy decreased as impact velocity increased, but it increased by an average of 8% when the plate surfaces were inclined. This phenomenon can be explained by the geometric nonlinearity in the ceramic plate, which changes the direction of movement of the projectile and causes differences in the damage formation in the target plates. The damages that occurred in ceramic plates were obtained through the fragment plotting method, and the ceramic plates were visualized to show the damage structures. The use of an inclined plate provides higher efficiency in alumina samples at high speeds, while the efficiency provided by the oblique surface decreases as the impact speed increases in silicon carbide and boron carbide plates.

Keywords: *Impact, Alumina, Silicon carbide, Boron carbide, Finite element, SPH*

1. Introduction

Ceramics stand out among many materials used for ballistic armor due to their low density and superior mechanical properties. The most commonly used ceramic materials in ballistic applications are alumina, silicon carbide, and boron carbide, but alumina stands out as the most widely used in terms of cost-performance [1–5]. While fracture toughness, hardness, bending and elastic modulus are seen as the most decisive properties for ballistic resistance, ceramics are quite successful in meeting these requirements with their mechanical properties [6]. On the other hand, reinforcing the front and back surfaces of ceramic plates with materials that have different properties increases their ballistic performance [7, 8]. Many different studies have been conducted on the ballistic resistance of ceramics [9]. The variables used in these studies can be listed as ceramic types, impactors with different geometries, impact velocities, ceramic plate thicknesses, and so on. Studies have shown that increasing the thickness of ceramic plates improves their strength, but the ballistic resistance decreases when using thinner plates. Blunt-nosed impactors distribute the impact better due to their broad contact area, making armor plates more resistant to such threats. On the other hand, pointed-nosed impactors penetrate structures more quickly due to their low initial contact area, transmitting the impact more intensely [10–13].

Reaugh et al. [13] conducted experiments to examine the performance of various materials when backed by thick ballistic steel against high-velocity impacts. They used a projectile with an aspect ratio of four, which combines the characteristics of short projectiles and long rods. Their results showed that silicon carbide, boron carbide, and titanium diboride perform well when backed by steel, outperforming aluminum nitride, Pyrex, and alumina at speeds under 2.0 km/s. Aluminum nitride performed best at speeds over 2.0 km/s, retaining its strength under high confining pressures. Pyrex ranked similarly to boron carbide, titanium diboride, and silicon carbide at 2.6 km/s and may even perform better at higher velocities. Rajagopal and Naik [14] developed an analytical model and performed experiments to study the behavior of thick composite structures under oblique ballistic impacts. The results were validated and showed that shear plugging is the primary energy-absorbing mechanism, followed by friction. The ballistic limit velocity varies depending on the thickness of the specimen and increases as the initial obliquity of contact decreases. Anderson et al. [15] conducted experiments to determine if the difference in penetration rates of two intact SiC-N data sets was due to a scaling impact of the rod diameter. They tested different rod diameters against bare and sleeved SiC-N cylinders at impact velocities between 2-3 km/s. They found that there was no scaling effect of penetration velocity for different rod diameters within data scatter. They also examined the analysis process used to determine penetration rates and found that older data aligned with newer data when analyzed in the same way. They discovered that there were no differences in the penetration rate for intact, pre-damaged, or in situ comminuted ceramic. The data scatter in the penetration velocity of SiC-N was likely due to variation in the failure dynamics of brittle material during penetration. The variability observed in penetration velocity as a function of impact velocity was the result of variability in failure dynamics as ceramic transitions from intact to failed material. Karabulut et al.[16] conducted a study on creating lightweight armor materials with improved ballistic performance. They used a new manufacturing technique that involved melting aluminum ingots and adding 8% by weight of B_4C, SiC, and Al_2O_3 particles individually. The resulting functionally graded materials (FGMs) were divided into four parts and hot-rolled to create laminated FGMs. The study examined the effects of reinforcement particles and fabrication techniques on density, microstructure, microhardness, and tensile strength. The ballistic resistances of the developed FGMs were also examined using a 7.62 mm M80 projectile. Results showed that the B_4C-reinforced laminated FGM provided the best ballistic protection, with the projectile halted at the second layer. Overall, the study demonstrated the potential of using centrifugal casting and hot rolling to create graded, lightweight ballistic armor materials.

Mamivand and Liaghat [17] developed an analytical model of a woven fabric that can predict its ballistic performance. The model accounts for dynamic material properties and stress attenuation in the fabric caused by wave reflection at warp and weft junctions. The model was found to be accurate in predicting the ballistic limit for multi-layer fibrous targets. The study also investigated the impact of layer spacing and target dimensions on ballistic performance. Results showed that cloth sheet dimensions are crucial to ballistic performance and there is a threshold for layer spacing beyond which increasing the spacing has little impact on the target's ballistic performance. The study also identified an area where target dimension has a significant impact on ballistic limit, which changes when different impact velocities are used on the same target. Finally, the study found that target size has no effect on ballistic performance for large targets where the transverse and longitudinal waves do not soon reach the boundary.

Feli and Asgari [18] propose a new FE simulation method for studying cylindrical projectile penetration into ceramic composite targets. They use the Johnson-Holmquist model to explain the fragmentation of the ceramic front plate, taking into account brittle failure, high pressure and strain rate effects, and deformation of the ceramic material under high-velocity impact. The study compares their findings on residual velocity and perforation time with those of other studies and investigates the effectiveness of ceramic or composite armor under ballistic impact. The results show that with increasing initial velocity of the projectile, the semi-angle of the fragmented ceramic conoid decreases, and the delamination of upper layers of the composite plate decreases. At initial velocities between 470 and 500 m/s, an increase in the computed residual velocity of the projectile is observed. Near the ballistic limit velocity, the projectile remains in the broken ceramic tile for a longer period of time, and the dishing of composite layers also increases. Gergori et al.[19] developed analytical and numerical models to simulate the impact of a projectile on ceramic composite targets for use in ballistic shields. While the simulations predicted higher residual velocities than the experiments, the ballistic limits were reliable. The analytical model showed higher residual velocities than the numerical model because it homogenized the projectile as a cylinder, whereas the numerical model included its actual core and jacket. However, the two approaches agreed well on the energies related to the main dissipation mechanisms. Meng et al.[20] reviewed the use of Smoothed Particle Hydrodynamics (SPH) for simulating high-velocity impact (HVI) over the past 30 years. They provide a brief introduction to SPH and its applications, followed by a discussion of the current state of SPH in HVI modeling, its limitations, and recent developments. The authors conclude that there is still a need for further research in developing SPH models for projectile-target systems. However, there have been several SPH formulations, including CSPM, Godunov SPH, complete Lagrangian SPH, and pseudo-springs SPH, that have improved the performance of SPH simulations for HVI problems. The SPH approach is also compatible with other algorithms and has been used to address a variety of HVI issues beyond metallic projectile-target systems. The accuracy of SPH in predicting fragmentation and debris clouds phenomena is due to its particle properties.

In this study, ceramic target plates were created with four different surface angles and three different ceramic materials, and four different initial velocity values were selected for the projectile. A total of 48 combinations of 4x3x4 parameters were analyzed as a result. In the established model, although the surface angles varied, the thickness of the ceramic plate at the point of impact was kept constant at 6 mm for all samples. Thus, the aim was to ensure that the effect of the change in slope angle on the damage to the plate was independent of the thickness at which the pressure wave progressed upon initial contact.

2. Materials and Methods

In this study, the finite element method was used to investigate the ballistic impact resistance of ceramic armors. Our model is a finite element model created with the smoothed particle hydrodynamics (SPH) method. This method models the material as interconnected small particles, and each particle interacts with other particles. Different strength models were used for ceramic, composite, and bullet materials. The Johnson-Holmquist model was used for ceramic materials (Al2O3, SiC, B4C), the Max Stress and Max Strain models were used for composite material (Aramid epoxy), and the Johnson-Cook strength model was used for projectile material (Steel 4340). This section will provide information on the materials and material models used, as well as the finite element model.

2.1. Projectile material

The Johnson-Cook model is used to predict the behavior of materials under high-speed impacts. This model considers material plastic deformation, melting point, and fracture, among other factors. The theoretical basis of this model includes the indication of the material's elastic and plastic deformation and stress-crack extension behavior. The parameters used for the Johnson-Cook model include yield strength, maximum stress, maximum compression, maximum crack extension, fracture strength, melting point, thermal expansion coefficient, thermal conductivity, and shear resistance.

The model for the von Mises tensile flow stress (σ) is expressed as [21];

$$\sigma = [A + B\varepsilon^n][1 + Cln\dot{\varepsilon}^*][1 - T^{*m}] \tag{1}$$

In this equation, A, B, C, m, and n denote the yield stress, hardening constant, strain rate constant, thermal softening constant and hardening exponent values, respectively. The expression for strain at the fracture (ε^f) is given as follows.

$$\varepsilon^f = \left[D_1 + D_2\, exp^{D_3\sigma^*}\right][1 + D_4 ln\dot{\varepsilon}^*][1 + D_5 T^*] \tag{2}$$

$$\sigma^* = \sigma_m / \overline{\sigma} \tag{3}$$

$$\dot{\varepsilon}^* = \frac{\dot{\varepsilon}}{\dot{\varepsilon}_0} \tag{4}$$

for $\dot{\varepsilon}_0 = 1.0\ s^{-1}$

$$T^* = \frac{(T - T_{room})}{T_{melt} - T_{room}} \tag{5}$$

The material properties used for Steel 4340 were taken from Johnson and Cook [19]. The Johnson-Cook strength parameters for Steel 4340 are given in Table 1.

Table 1. Johnson-Cook strength parameters of steel 4340

Parameter	**Value**	**Unit**
Reference density	7.83	g/cm³
Shear Modulus	77	GPa
Yield Stress **(A)**	792	MPa
Hardening Constant **(B)**	510	MPa
Hardening Exponent **(n)**	0.26	-
Strain Rate Constant **(C)**	0.014	-
Thermal Softening Exponent **(m)**	1.03	-
Damage Constant **(D1)**	0.05	-
Damage Constant **(D2)**	3.44	-
Damage Constant (**D3)**	-2.12	-
Damage Constant **(D4)**	0.002	-
Damage Constant **(D5)**	0.61	-
Melting Temperature	1793	K
Ref. Strain Rate (/s)	1	-

2.2. Ceramics

The ceramic material models were defined using the Johnson-Holmquist (JH-2) model. The Johnson-Holmquist model is a material model used to model the behavior of materials under high-speed impact loads. This model considers material stress-crack extension behavior, high-speed plastic deformation, and material fracture, among other factors. The theoretical basis of this model consists of three different sections created separately for compression and stress conditions: the elastic region, the plastic region, and the fracture region. The material behavior is defined differently for each of these regions. The normalized equivalent stress (σ^*), normalized intact equivalent stress (σ_i^*), and normalized fracture stress (σ_f^*) are given by the following equations [20, 21],

$$\sigma^* = \sigma_i^* - D\left(\sigma_i^* - \sigma_f^*\right) \tag{6}$$

$$\sigma^* = \sigma/\sigma_{HEL} \tag{7}$$

$$\sigma_f^* = [B(P^*)^M][1 + Cln\varepsilon^*] \tag{8}$$

$$\sigma_i^* = [A(P^* + T^*)^N][1 + Cln\varepsilon^*] \tag{9}$$

In this equation, σ_{HEL} and D present the equivalent stress at Hugoniot elastic limit (HEL) and damage (0 < D < 1), respectively.

$$D = \sum \frac{\Delta\varepsilon_p + \Delta\mu_p}{\varepsilon_p^f + \mu_p^f} \tag{10}$$

Damage was calculated by Eq. (10), where $\Delta\varepsilon_p$ and $\Delta\mu_p$ are equivalent plastic strain and plastic volumetric strain, respectively. Under a constant pressure P, the plastic strain to fracture is given as,

$$\varepsilon_p^f + \mu_p^f = D1(P^* + T^*)^{D2} \tag{11}$$

In this equation, D1 and D2 are damage constants. P^* and T^* are expressed as follows,

$$P^* = P/P_{HEL} \tag{12}$$

$$T^* = T/P_{HEL} \tag{13}$$

In these equations, P and T are the initial pressure and maximum tensile hydrostatic tensile pressure that the material can withstand, while P^* and T^* respectively represent the normalized pressure and normalized maximum tensile hydrostatic pressure. Damages are accumulated by the Johnson-Cook fracture model from both volumetric and equivalent plastic strain.

The first section is the linear elastic zone ($P \leq Pcrush$), while the second is the transition region where the material's air spaces are gradually forced out, causing plastic volumetric strain ($P_{crush} \leq P \leq P_{lock}$). The third region represents fully dense material, and pressure reaches $Plock$, expressed as Eq. 14. μ= modified volumetric strain. K1, K2, and K3 are constants equivalent to those used for material with no void.

$$P = K1\bar{\mu} + K2\bar{\mu}^2 + K3\bar{\mu}^3 \tag{14}$$

$$\bar{\mu} = \frac{\mu - \mu_{lock}}{1 + \mu_{lock}} \tag{15}$$

The material properties used for ceramic materials were taken from previous works [22–24]. Table 2 gives the Johnson-Holmquist (JH-2) strength parameters for Alumina, Silicon carbide, and boron carbide.

Table 2. Johnson Holmquist (JH-2) strength parameters.

Parameter	**Value**			**Unit**
	Alumina (Al_2O_3)	Silicon Carbide (SiC)	Boron Carbide (B_4C)	
Reference density	3.7	3.215	2.51	g/cm^3
Bulk Modulus	130.95	220	233	GPa
Shear Modulus	90.16	193	197	GPa
Hugoniot Elastic Limit	19	11.7	19	GPa
Intact Strength Constant **(A)**	0.93	0.96	0.987	-
Intact Strength Exponent **(N)**	0.6	0.65	0.67	-
Strain Rate Constant **(C)**	0.007	0.009	0.005	-
Fractured Strength Constant **(B)**	0.31	0.35	0.7	-
Fractured Strength Exponent **(M)**	0.6	1	0.85	-
Max. Fracture Strength Ratio	0.2	0.2	0.2	-
Hydro Tensile Limit	1.46	0.750	0.260	GPa
Damage Constant **(D1)**	0.005	0.02	0.001	-
Damage Constant **(D2)**	1	1.85	0.5	-
Bulking Constant, Beta	1	1	1	-

2.3. Composite

Maximum stress-strain models were used for composite materials. The max-stress model calculates the maximum stress value of the composite material and assumes linear behavior until reaching the breaking point. The max-strain model calculates the maximum deformation value and assumes linear behavior until reaching the breaking point. Definitions for delamination, fiber damage, and matrix damage are provided in the following equations(Software product, n.d.).

Delamination,

$$e_{11f}^2 = \left(\frac{\sigma_{11}}{X_T}\right)^2 + \left(\frac{\sigma_{12}}{S_{12}}\right)^2 + \left(\frac{\sigma_{31}}{S_{31}}\right)^2 \geq 1 \tag{16}$$

Fiber Failure,

$$e_{22f}^2 = \left(\frac{\sigma_{22}}{Y_T}\right)^2 + \left(\frac{\sigma_{12}}{S_{12}}\right)^2 + \left(\frac{\sigma_{23}}{S_{23}}\right)^2 \geq 1 \tag{17}$$

Matrix cracking,

$$e_{33f}^2 = \left(\frac{\sigma_{33}}{Y_T}\right)^2 + \left(\frac{\sigma_{23}}{S_{23}}\right)^2 + \left(\frac{\sigma_{31}}{S_{31}}\right)^2 \geq 1 \tag{18}$$

Aramid epoxy material properties are taken from the previous work of Tepeduzu and Karakuzu [22] and are shown in Table 3.

Table 3. Mechanical properties of aramid epoxy composite.

Parameter	Value	Unit
Density	1117	kg/m3
Elastic Modulus-Longitudinal **(E_{11})**	17230	MPa
Elastic Modulus-Transverse **(E_{22})**	17230	MPa
Elastic Modulus-Normal **(E_{33})**	10340	MPa
Poisson's Ratio **(ν_{23})**	0.12	–
Poisson's Ratio **(ν_{31})**	0.12	–
Poisson's Ratio **(ν_{12})**	0.2	–
Tensile Strength-Longitudinal **(X_t)**	425	MPa
Compressive Strength-Longitudinal **(X_c)**	88	MPa
Tensile Strength-Transverse **(Y_t)**	425	MPa
Compressive Strength-Transverse **(Y_c)**	88	MPa
Tensile Strength-Normal **(Z_t)**	255	MPa
Compressive Strength-Normal **(Z_c)**	53	MPa
Shear Modulus-Transverse **(G_{23})**	3300	MPa
Shear Modulus-Transverse **(G_{31})**	3300	MPa
Shear Modulus-In plane **(G_{12})**	5510	MPa
Shear Strength-Transverse **(S_{23})**	40	MPa
Shear Strength-Transverse **(S_{31})**	40	MPa
Shear Strength-In plane **(S_{12})**	66	MPa

2.4. Finite Element Model

The finite element model was created using the SPH method. The SPH method uses interacting particles to model a system. Each particle has properties such as mass, position, and velocity, which are calculated at an "interaction point." The interaction region around this point is defined by neighboring particles and their distances. Interaction functions determine how these particles interact, based on their distances and coefficients. This method provides flexibility and precision in modeling solid mechanics, particularly fluid behaviors.

Here, the projectile, ceramic plate, and composite plate were modeled using the SPH method with an ANSYS Autodyn nonlinear dynamics analysis solver. A total of 198939 SPH elements were used in the model. The M61 7.62x51 mm armor-piercing ammunition geometry was used for the projectile. Ceramic plates with dimensions of 40x40x6 mm and composite plates with dimensions of 300x300x10 mm were created. Three different ceramics were defined for the ceramic plate, namely alumina, silicon carbide, and boron carbide, and Aramid-epoxy materials were defined for the backing composite plate.

To verify the accuracy of the finite element model, the analyses conducted by Tepeduzu and Karakuzu [22] using aramid epoxy and alumina were repeated in this model, and reasonably accurate results were obtained. Similar to mesh convergence studies in traditional FEM, particle spacing sensitivity was also investigated in the SPH simulations to ensure numerical accuracy. Several simulations were conducted using different particle spacing values, and the resulting residual velocities and damage patterns were compared. The selected particle spacing provided a good balance between computational efficiency and result fidelity, with deviations remaining below 6% when compared to literature-based benchmark data. This confirms that the model resolution was sufficient for capturing the essential impact behavior without excessive computational cost. The results are presented in Table 4.

Table 4. Reference vs. present study residual impact velocities.

	Impact velocity (m/s)	700	750	800	850
Residual velocity (m/s)	Reference	496	562	612	652
	Present	526	567	609	645

In this study, ceramic target plates were created with four different surface angles and three different ceramic materials. Four different velocity values were selected for the projectile's initial velocity. As a result, analyses were performed with a total of 48 combinations from 4x3x4 parameters. In the established model, although the surface angles varied, the thickness at which the projectile hit the ceramic plate was kept constant at 6 mm for all samples. Thus, it was aimed that the effect of the change in the slope angle on the damage to the plate would be independent of the thickness at which the pressure wave progressed at the initial contact. The projectile initial velocity was selected as 500, 750, 1000, and 1250 m/s. The schematic view of the designed model and the selected section dimensions for ceramics are given in Figure 1 and Table 5, respectively. The main difference of this study from previous studies is the approach used, as well as the evaluation of the three different ceramic materials frequently used in armor structures with different velocities and impact angles in the same study.

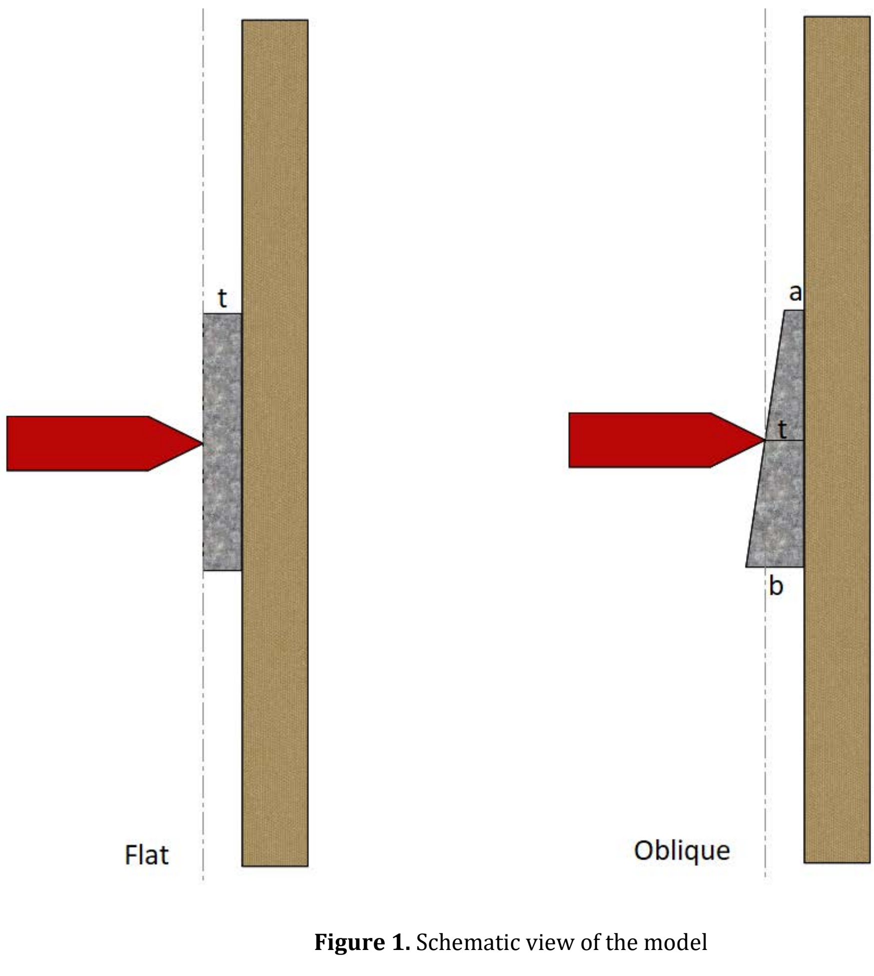

Figure 1. Schematic view of the model

The parameters used in the model are provided in Table 5. In this study, the effective thickness of the ceramic plates was kept constant at 6 mm for all configurations to ensure that the resistance offered in the impact direction remained consistent. The inclined geometries (Ob1–Ob3) were designed accordingly, which resulted in relatively small surface angles (2.86°, 5.71°, and 8.53°). Selecting larger angles would have required significantly thicker ceramic geometries to preserve the same effective thickness, leading to an increase in computational cost and reduced experimental feasibility. Furthermore, the inclined plate geometry was applied only to the ceramic layer; the backing composite plate remained flat relative to the projectile's trajectory. This setup ensured that the observed residual velocities predominantly reflected the behavior of the ceramic plates alone, avoiding additional variability introduced by changes in the effective thickness of the backing plate.

Table 5. Section properties of the models

	Dimensions			
	a (mm)	b (mm)	t (mm)	Angle (θ)
Flat	6	6	6	0
Oblique 1 (Ob1)	5	7	6	2.86
Oblique 2 (Ob2)	4	8	6	5.71
Oblique 3 (Ob3)	3	9	6	8.53

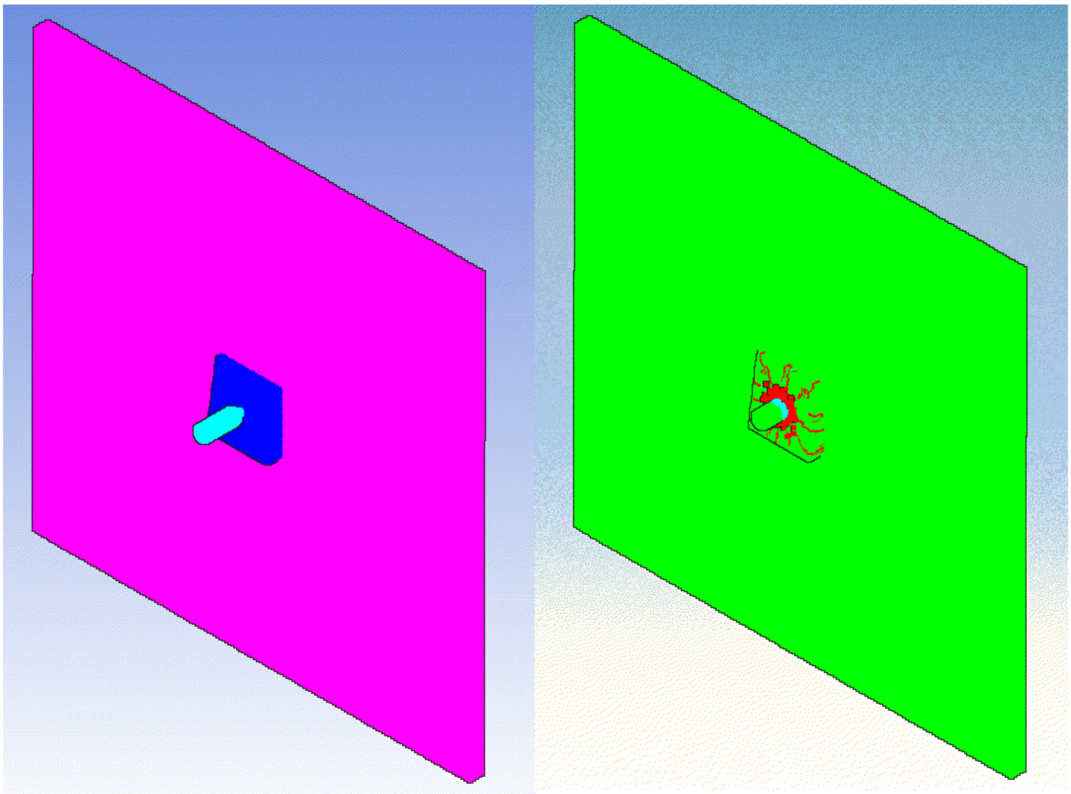

Figure 2. Finite element model of the impact procedure.

3. Results and Discussion

In this study, three different ceramic materials were modeled with different surface angles and subjected to impact loading at different velocities. The projectile residual velocity, absorbed energy values, and damage data on the plates were obtained using the results of finite element analysis. Figures 3-5 show the projectile impact and residual velocity values for different surface angles of alumina, silicon carbide, and boron carbide samples, respectively.

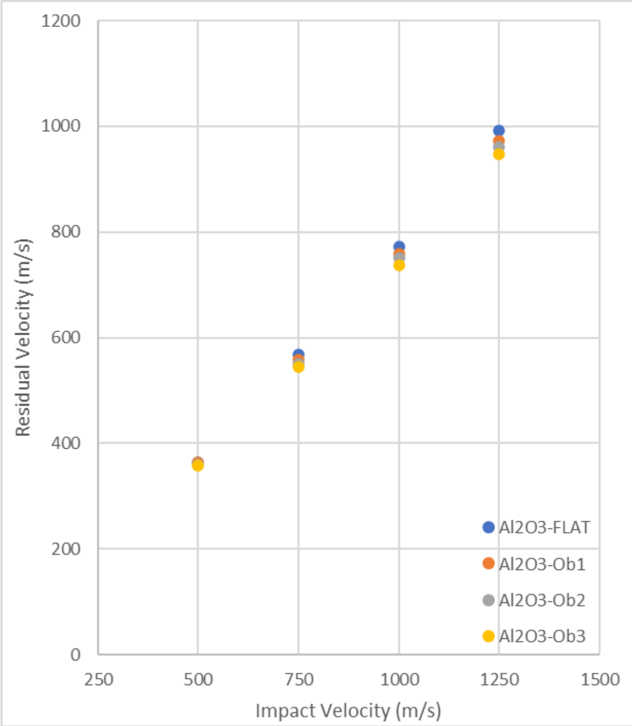

Figure 3. Impact and residual velocities of a projectile on the alumina target

When looking at the overall impact performance, both boron carbide and silicon carbide showed better impact performance among these samples. It is observed that the increase in surface angle reduces the projectile residual velocity from the target plate. This decrease in residual velocity due to the rise in surface angle is seen in all impact velocities for the boron carbide sample, while significant decreases were observed in high-speed impact analyses for alumina and silicon carbide samples, and no significant differences were observed in low-speed analyses. We can say that this effect occurs depending on the hardness and strain rates of the ceramic plates used. As the impact velocity increases, the response time of the plates decreases, and they exhibit a more rigid character. As a result, the deformation and direction change of the projectile hitting the inclined surface of the plate occur at a higher rate in high-speed impacts.

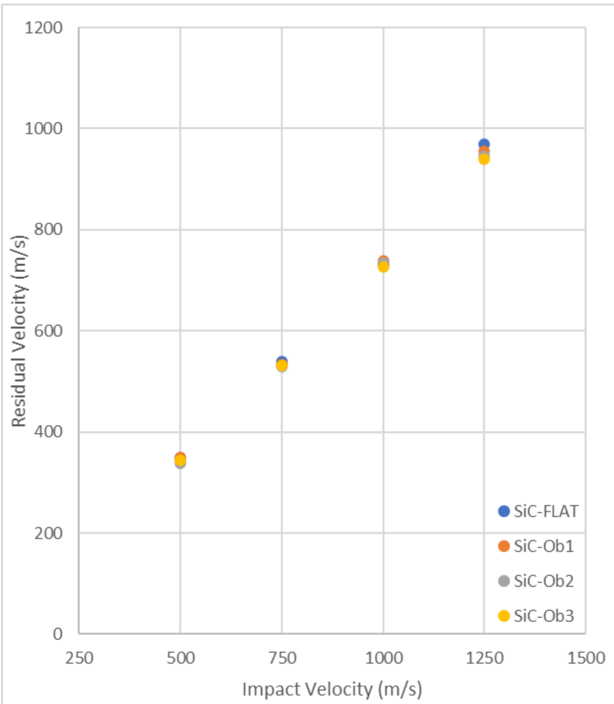

Figure 4. Impact and residual velocities of a projectile on a silicon carbide target

The boron carbide plate exhibits this effect from low speeds due to its high hardness and low deformation rate. For alumina and silicon carbide, it was expected that silicon carbide would have a more significant response to the increase in impact velocity and surface angle considering the hardness values of the plates, while higher differences were observed in the alumina plate. This result shows that the deformation rate under high-speed impact conditions has a more dominant effect on the material's impact performance.

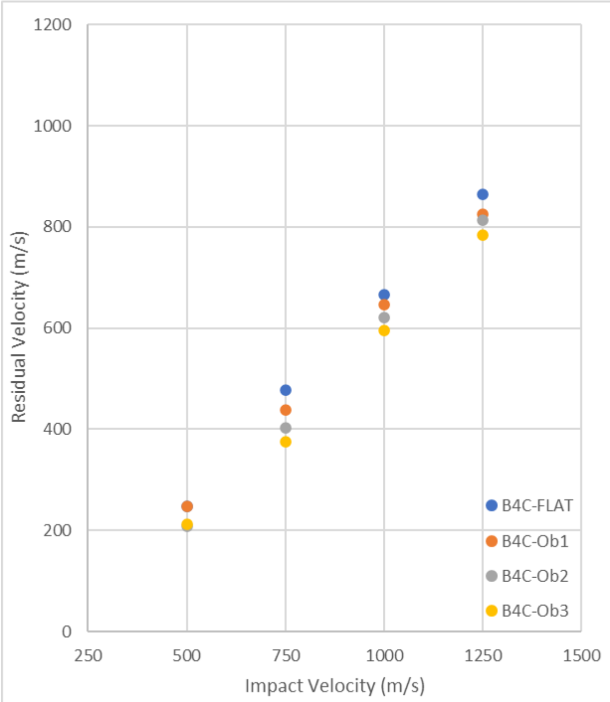

Figure 5. Impact and residual velocities of a projectile on a boron carbide target

Figure 6 presents a clustered heatmap that visualizes the exit velocities recorded for each specimen under different impact velocities (500–1250 m/s). Lower exit velocities indicate a higher capacity of the material to absorb kinetic energy, thus signifying better ballistic performance. Among the three material systems examined (Al_2O_3, SiC, and B_4C), B_4C-based specimens consistently exhibited the lowest exit velocities across all impact scenarios, confirming its superior energy absorption capability. Notably, the B4C-Ob3 specimen recorded the lowest overall values, followed closely by B4C-Ob2 and B4C-Flat, indicating that even the flat configuration of B_4C outperforms other materials with optimized geometries. SiC specimens demonstrated intermediate performance. While SiC-Flat provided reasonably low exit velocities, the addition of oblique geometries (Ob1–Ob3) resulted in marginal improvements. This suggests that although SiC inherently possesses decent ballistic resistance, geometric enhancements offer limited additional benefit compared to B_4C. On the other hand, Al_2O_3 specimens exhibited the highest exit velocities, especially in the flat configuration. However, a clear trend of performance improvement was observed with increasing geometric complexity. Al_2O_3-Ob3 showed a significant reduction in exit velocity compared to Al_2O_3-Flat, underscoring the importance of architectural design in enhancing relatively weaker ceramics.

From a design perspective, material selection has a dominant effect on ballistic performance, while geometric modifications can be particularly impactful when applied to materials with lower intrinsic strength. These findings align with the hierarchical clustering observed in the heatmap, where specimens naturally group according to material type and performance similarities.

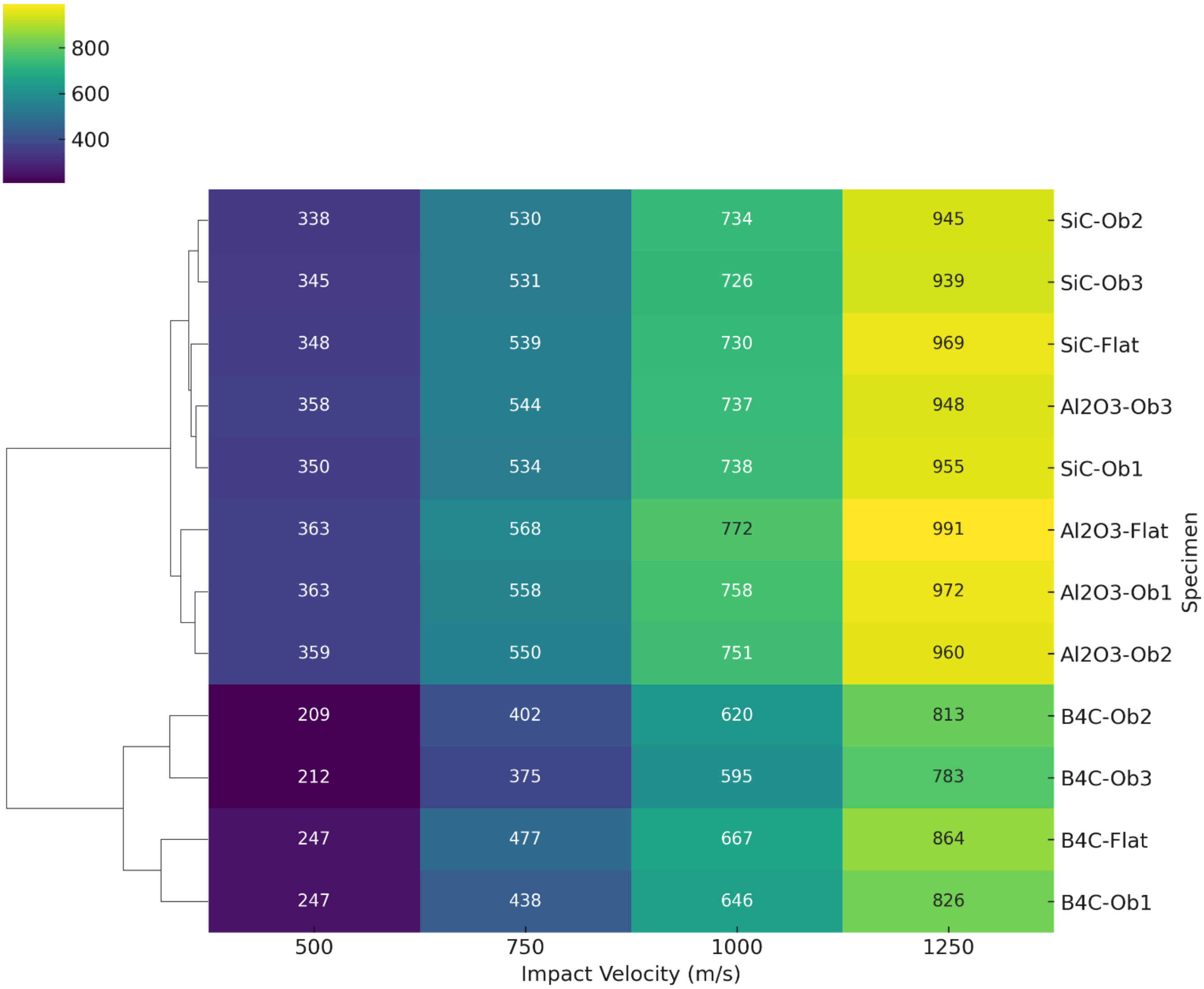

Figure 6. Clustered heatmap of exit velocities for different impact velocities and targets

Figure 7 provides the percentages of absorbed energy for all analysis combinations. When the energies absorbed by plates were examined, it was observed that the amount of absorbed energy decreased for all plates as the impact velocity increased (Fig. 7). Among the ceramics that were used, it can be said that boron carbide (B_4C) samples showed more dramatic decreases in the energy they absorbed. Especially in the case of the B_4C-flat sample, while it absorbed 74.6% of the energy at a 500 m/s impact velocity, the percentage of absorbed energy decreased to 60% at a 750 m/s impact velocity. When the plate surfaces were inclined, the amount of absorbed energy, which showed a tendency to decrease at high velocities, increased by an average of 8%.

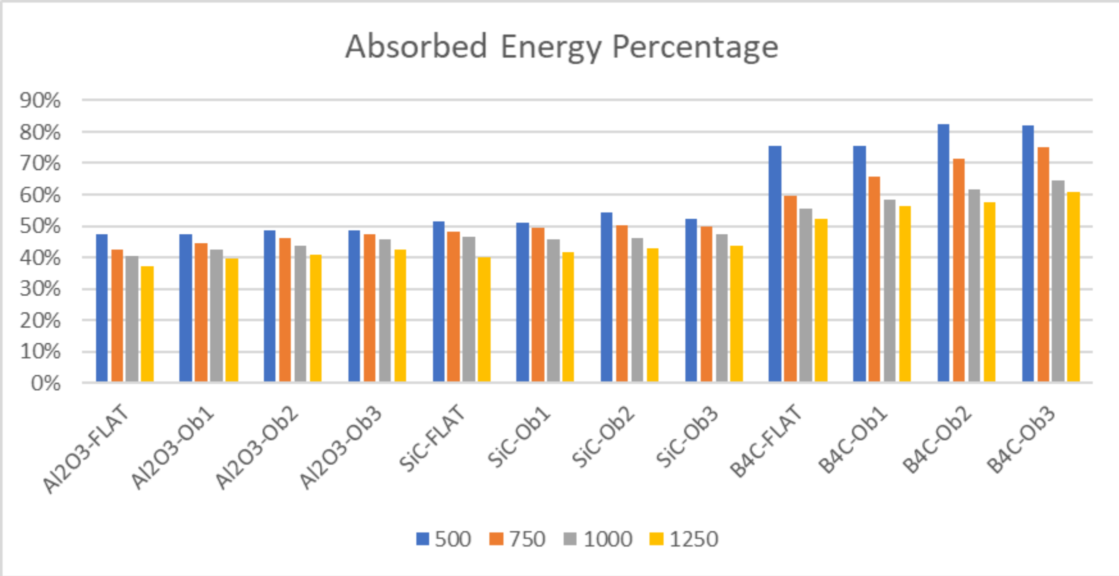

Figure 7. Absorbed energy percentage of all combinations

To explain this phenomenon, we first need to explain why the amount of absorbed energy decreases as the impact velocity increases. The amount of absorbed energy is directly related to the duration of the impact event. This duration is what increases the absorbed energy during the impact. Increasing this duration is related to the mechanical and geometric properties of the material used. Slowing down the projectile, causing structural deformation, reducing its fragility, and changing its direction prolongs this duration and indirectly increases the amount of absorbed energy.

Since high-speed impact is a highly complex nonlinear process that involves many different parameters, the effects mentioned here will not create linear results. However, increasing the impact velocity will fundamentally accelerate the process and decrease the amount of absorbed energy. On the other hand, the amount of absorbed energy increases with increasing surface angle. The thickness of all samples is 6 mm at the point where the projectile hits the ceramic plate, with no difference in thickness. This increase in absorbed energy due to inclined surfaces can be explained more precisely by the concept of momentum deflection angle. When the projectile impacts an inclined ceramic plate, the momentum vector of the projectile does not align with the surface normal, causing a directional deviation. This deviation leads to an altered interaction geometry, which increases the contact duration and energy dissipation. This effect, which constitutes a form of geometric nonlinearity, significantly changes the stress distribution and fragmentation path within the ceramic plate under high-velocity impact. In this case, the reason for the change in absorbed energy is the geometric nonlinearity in the ceramic plate, which changes the direction of movement of the projectile and causes differences in the damage formation in the target plates.

In a flat plate, the pressure wave is evenly transmitted along the ceramic width during the collision, while in inclined plates, higher contact forces occur at the thicker parts of the cross-section, and the projectile is directed towards the thinner section of the plate accordingly. This increases the distance the bullet penetrates within the cross-section. On the other hand, as a result of this deformation, the tip of the bullet becomes blunt, allowing the impact to be absorbed over a wider area on the ceramic, and thus, the damage area expands, dissipating more energy.

At the end of the analysis, the damages that occurred in ceramic plates were obtained through the fragment plotting method, and the elements that experienced bulk damage were removed; the ceramic plates were visualized in Figure 8. When the resulting damaged structures were examined, a diagonal main crack and micro-cracks were observed in the flat plate (Alumina-flat). In the oblique plate (Alumina Ob-3), it is seen that diagonal cracks widen in the section where the cross-section is narrowed, and the density of micro-cracks increases. In addition, the formation of the main crack is also observed along the vertical axis. These types of cracks occur as a result of the ceramic plate being forced to bend. This situation shows that the inclined plate exhibits a more rigid character, and the bending rigidity of the composite backing plate becomes important in the formation of damage. Indeed, in the silicon carbide sample, which has a more rigid structure than alumina, the main cracks occur in horizontal and vertical axes, while diagonal cracks are limited. In the boron carbide sample, the main cracks occur in the horizontal and vertical axes and are completely due to bending stress. The use of an inclined plate provides higher efficiency in alumina samples at high speeds, while the efficiency provided by the oblique surface decreases as the impact speed increases in silicon carbide and boron carbide plates. This situation can be explained by the bending stress. In these plates with high penetration resistance, after a threshold speed value, the bending rigidity of the backing plate becomes more prominent.

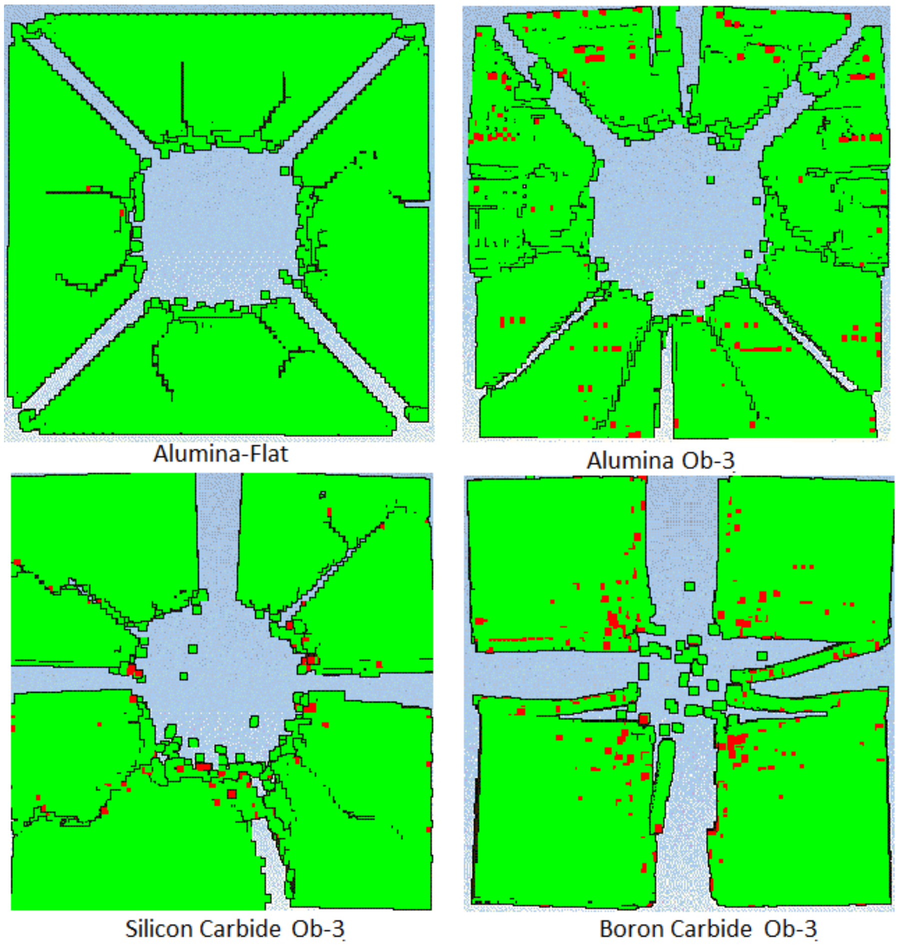

Figure 8. Fragment plot of the ceramic plates

In Figures 9 and 10, the damages that occurred in composite backing plates are given. The damaged areas in the composite plates behind the oblique ceramic plates are higher than those in the flat plates, indicating an increase in the amount of absorbed energy. Since the lower parts of the inclined plates are thicker, the contact forces have been higher in these regions, and it is observed that the damaged areas of the composites are more concentrated in the lower parts. The fiber damages in the front face were also observed in the silicon carbide and especially boron carbide sample analyses, as well as the cross in the back surface of the composite plates. This is due to the plates being subjected to higher levels of bending.

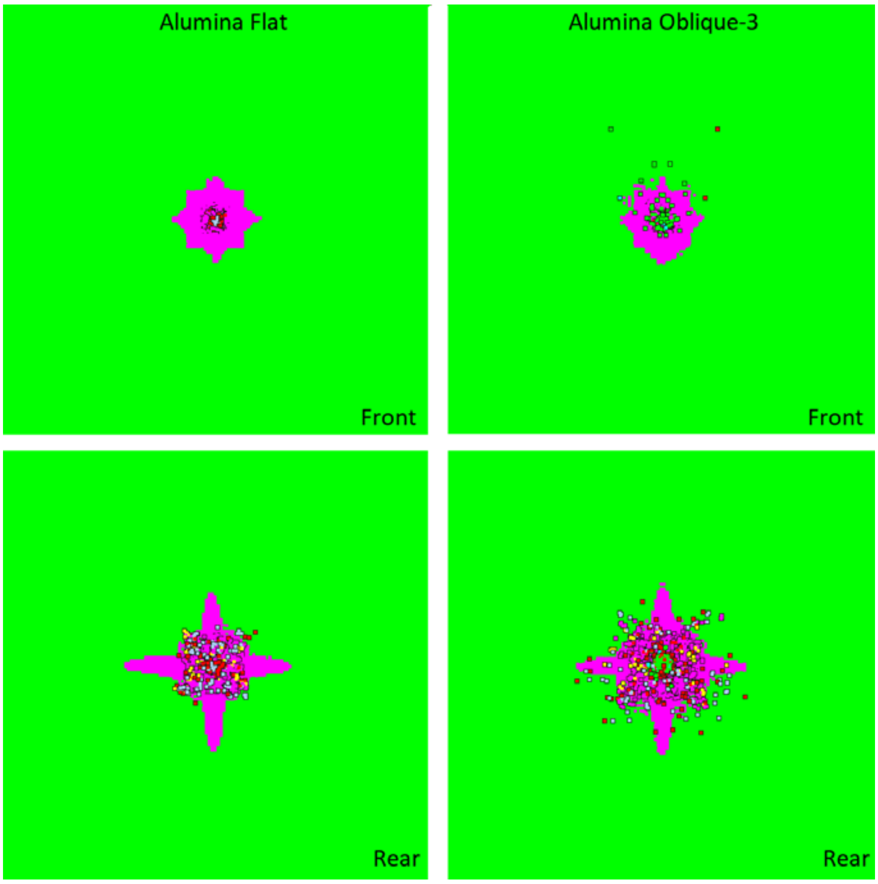

Figure 9. Damage view of composite backing plates (Flat/Oblique)

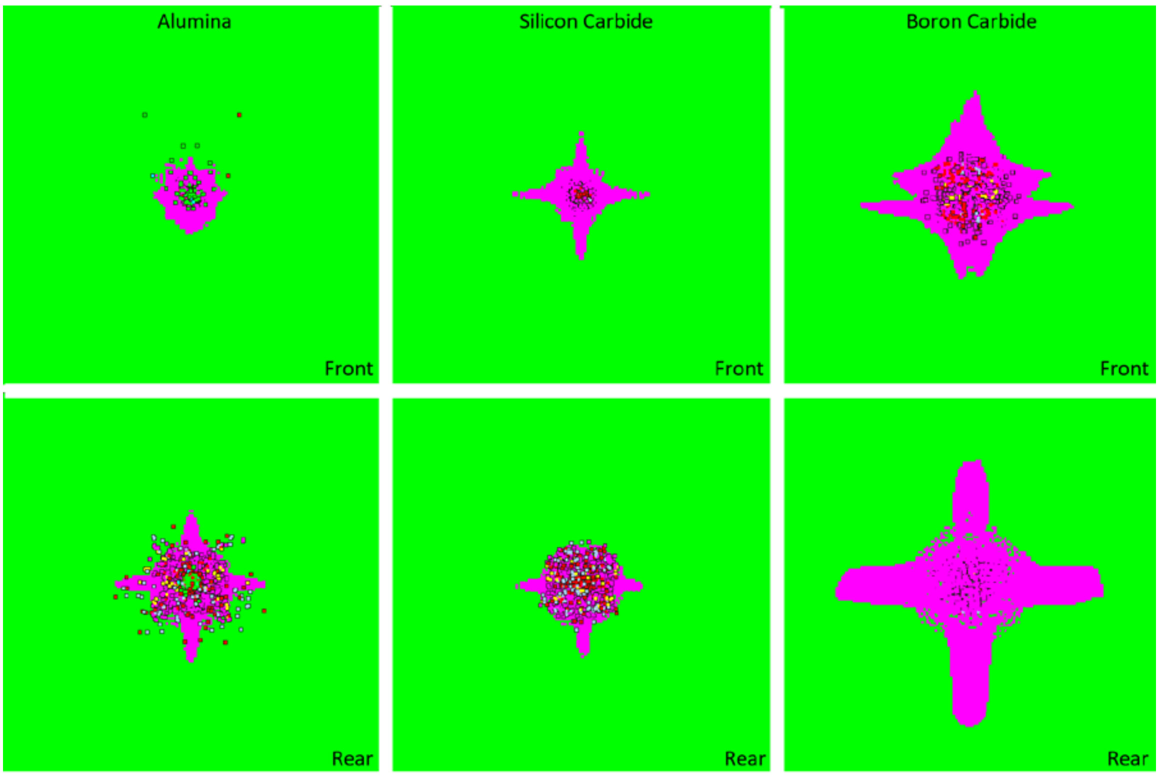

Figure 10. Damage view of composite backing plates with different frontier targets (Oblique)

4. Conclusions

The study discussed the impact performance of three different ceramic materials (alumina, silicon carbide, and boron carbide) with different surface angles when subjected to impact loading at different speeds. Finite element analysis is used to obtain the projectile residual velocity, absorbed energy values, and damage data on the plates. The boron carbide and silicon carbide samples showed better impact performance compared to alumina, with boron carbide being the most effective due to its high hardness and low deformation rate. The amount of absorbed energy decreased as the impact velocity increased for all plates, with boron carbide samples showing the most significant decreases. However, the amount of absorbed energy increased as the surface angle increased, which was attributed to geometric nonlinearity in the ceramic plates. The damaged structures observed in the ceramic plates showed diagonal main cracks and micro-cracks in the flat plate, while diagonal cracks widened in the section where the cross-section was narrowed, and the density of micro-cracks increased in the oblique plate. The silicon carbide sample exhibited main cracks in horizontal and vertical axes, while the boron carbide sample showed main cracks in the horizontal and vertical axes, and occurred entirely due to bending stress. The findings of this study provide valuable insights for armor optimization, as they offer guidance in selecting appropriate ceramic materials and surface configurations to maximize energy absorption and minimize projectile residual velocity under varying impact conditions.

Ethics committee approval and conflict of interest statement

This article does not require ethics committee approval.

This article has no conflicts of interest with any individual or institution.

Author Contribution Statement

Volkan ARIKAN is the sole author in designing and planning the analysis, preparing the models, performing the analysis, interpreting the results obtained, and writing the manuscript.

References

[1] A. B. Dresch, J. Venturini, S. Arcaro, O. R. K. Montedo, and C. P. Bergmann, “Ballistic ceramics and analysis of their mechanical properties for armour applications: A review,” Ceram. Int., vol. 47, no. 7, pp. 8743–8761, Apr. 2021, doi: 10.1016/j.ceramint.2020.12.095.

[2] G. J. Appleby-Thomas, D. C. Wood, A. Hameed, J. Painter, and B. Fitzmaurice, “On the effects of powder morphology on the post-comminution ballistic strength of ceramics,” Int. J. Impact Eng., vol. 100, pp. 46–55, Feb. 2017, doi: 10.1016/j.ijimpeng.2016.10.008.

[3] X. Guo, X. Sun, X. Tian, G. J. Weng, Q. D. Ouyang, and L. L. Zhu, “Simulation of ballistic performance of a two-layered structure of nanostructured metal and ceramic,” Compos. Struct., vol. 157, pp. 163–173, Dec. 2016, doi: 10.1016/j.compstruct.2016.08.025.

[4] J. P. Iii, “The rate-dependent fracture toughness of silicon carbide- and boron carbide-based ceramics,” J. Eur. Ceram. Soc., 2015.

[5] L. M. Bresciani, A. Manes, and M. Giglio, “An analytical model for ballistic impacts against ceramic tiles,” Ceram. Int., vol. 44, no. 17, pp. 21249–21261, Dec. 2018, doi: 10.1016/j.ceramint.2018.08.172.

[6] D. Hu, Y. Zhang, Z. Shen, and Q. Cai, “Investigation on the ballistic behavior of mosaic SiC/UHMWPE composite armor systems,” Ceram. Int., vol. 43, no. 13, pp. 10368–10376, Sep. 2017, doi: 10.1016/j.ceramint.2017.05.071.

[7] I. G. Crouch, M. Kesharaju, and R. Nagarajah, “Characterisation, significance and detection of manufacturing defects in reaction sintered silicon carbide armour materials,” Ceram. Int., vol. 41, no. 9, pp. 11581–11591, Nov. 2015, doi: 10.1016/j.ceramint.2015.06.083.

[8] S. G. Savio and V. Madhu, “Ballistic performance evaluation of ceramic tiles with respect to projectile velocity against hard steel projectile using DOP test,” Int. J. Impact Eng., vol. 113, pp. 161–167, Mar. 2018, doi: 10.1016/j.ijimpeng.2017.11.020.

[9] Defence Metallurgical Research Laboratory, Hyderabad, S. G. Savio, V. Madhu, and A. K. Gogia, “Ballistic performance of alumina and zirconia-toughened alumina against 7.62 armour piercing projectile,” Def. Sci. J., vol. 64, no. 5, pp. 477–483, Sep. 2014, doi: 10.14429/dsj.64.6745.

[10] “An experimental study on ballistic performance of boron carbide tiles,” Int. J. Impact Eng., vol. 38, no. 7, pp. 535–541, Jul. 2011, doi: 10.1016/j.ijimpeng.2011.01.006.

[11] “Impact studies of five ceramic materials and pyrex,” Int. J. Impact Eng., vol. 23, no. 1, pp. 771–782, Dec. 1999, doi: 10.1016/S0734-743X(99)00121-9.

[12] A. Rajagopal and N. Naik, “Oblique ballistic impact behavior of composites,” Int. J. Damage Mech., vol. 23, pp. 453–482, Apr. 2013, doi: 10.1177/1056789513499268.

[13] C. E. Anderson, T. Behner, T. J. Holmquist, and D. L. Orphal, “Penetration response of silicon carbide as a function of impact velocity,” Int. J. Impact Eng., vol. 38, no. 11, pp. 892–899, Nov. 2011, doi: 10.1016/j.ijimpeng.2011.06.002.

[14] Ş. Karabulut, H. Karakoç, M. Bilgin, H. Canpolat, G. M. Krolczyk, and M. Sarıkaya, “A comparative study on mechanical and ballistic performance of functionally graded Al6061 composites reinforced with B4C, SiC, and Al2O3,” J. Mater. Res. Technol., vol. 23, pp. 5050–5065, Mar. 2023, doi: 10.1016/j.jmrt.2023.02.116.

[15] M. Mamivand and G. H. Liaghat, “A model for ballistic impact on multi-layer fabric targets,” Int. J. Impact Eng., vol. 37, no. 7, pp. 806–812, Jul. 2010, doi: 10.1016/j.ijimpeng.2010.01.003.

[16] S. Feli and M. R. Asgari, “Finite element simulation of ceramic/composite armor under ballistic impact,” Compos. Part B Eng., vol. 42, no. 4, pp. 771–780, Jun. 2011, doi: 10.1016/j.compositesb.2011.01.024.

[17] D. Gregori, R. Scazzosi, S. G. Nunes, S. C. Amico, M. Giglio, and A. Manes, “Analytical and numerical modelling of high-velocity impact on multilayer alumina/aramid fiber composite ballistic shields: Improvement in modelling approaches,” Compos. Part B Eng., vol. 187, p. 107830, Apr. 2020, doi: 10.1016/j.compositesb.2020.107830.

[18] S. Meng, L. Taddei, N. Lebaal, and S. Roth, “Advances in ballistic penetrating impact simulations on thin structures using Smooth Particles Hydrodynamics: A state of the art,” Thin-Walled Struct., vol. 159, p. 107206, Feb. 2021, doi: 10.1016/j.tws.2020.107206.

[19] G. R. Johnson and W. H. Cook, “Fracture characteristics of three metals subjected to various strains, strain rates, temperatures and pressures,” Eng. Fract. Mech., vol. 21, no. 1, pp. 31–48, Jan. 1985, doi: 10.1016/0013-7944(85)90052-9.

[20] G. R. Johnson and T. J. Holmquist, “An improved computational constitutive model for brittle materials,” in AIP Conference Proceedings, Colorado Springs, Colorado (USA): AIP, 1994, pp. 981–984. doi: 10.1063/1.46199.

[21] T. J. Holmquist, G. R. Johnson, and W. H. Cook, “A computational constitutive model for concrete subjected to large strains, high strain rates, and high pressures,” 14th Int. Symp. Vol 2 Warhead Mech. Termin. Ballist. 1993 Quebec Can., pp. 591–600, Jan. 1993.

[22] B. Tepeduzu and R. Karakuzu, “Ballistic performance of ceramic/composite structures,” Ceram. Int., vol. 45, no. 2, pp. 1651–1660, Feb. 2019, doi: 10.1016/j.ceramint.2018.10.042.

[23] L. Chandran, S. D. Rapaka, K. Eswara Prasad, and R. K. Annabattula, “Modeling the failure of silicon carbide under high strain-rate compression: A parametric study,” Mater. Today Proc., p. S2214785323012099, Mar. 2023, doi: 10.1016/j.matpr.2023.03.167.

[24] L. Westerling, P. Lundberg, and B. Lundberg, “Tungsten long-rod penetration into confined cylinders of boron carbide at and above ordnance velocities,” Int. J. Impact Eng., 2001.

[25] Software product, “Autodyn Composite Modeling Guide,” ANSYS 2019.